Journal of Medicinal Chemistry

Brief Article

Michael Acceptor-Based Peptidomimetic Inhibitor of Main Protease from Porcine Epidemic Diarrhea Virus

Fenghua Wang, Cheng Chen, Kailin Yang, Yang Xu, Xiaomei Liu, Fan Gao, He Liu, Xia Chen, Qi Zhao, Xiang Liu, Yan Cai, and Haitao Yang

J. Med. Chem., **Just Accepted Manuscript** • DOI: 10.1021/acs.jmedchem.7b00103 • Publication Date (Web): 13 Mar 2017

ACS Publications

Journal of Medicinal Chemistry is published by the American Chemical Society. 1155 Sixteenth Street N.W., Washington, DC 20036

Michael Acceptor-Based Peptidomimetic Inhibitor of Main Protease from Porcine Epidemic Diarrhea Virus

Fenghua Wang,[†,+] Cheng Chen,[†,‡,+] Kailin Yang,[#,+] Yang Xu,[‡] Xiaomei Liu,[‡] Fan Gao,[‡] He Liu,[‡] Xia Chen,[†] Qi Zhao,[§] Xiang Liu,[‡] Yan Cai,[‡,*] and Haitao Yang[†,‡,*]

[†]School of Life Sciences, Tianjin University, Tianjin 300072, China
[‡]Tianjin International Joint Academy of Biotechnology and Medicine, Tianjin 300457, China
[#]Cleveland Clinic Lerner College of Medicine of Case Western Reserve University, Cleveland, Ohio 44195, United States
[§]Department of Molecular Biophysics and Biochemistry, Yale University, New Haven, Connecticut 06520, United States

ABSTRACT: Porcine epidemic diarrhea virus (PEDV) causes high mortality in pigs. PEDV main protease (M^{pro}) plays an essential role in viral replication. We solved the structure of PEDV M^{pro} complexed with peptidomimetic inhibitor N3 carrying a Michael acceptor warhead, revealing atomic level interactions. We further designed a series of 17 inhibitors with altered side groups. Inhibitors M2 and M17 demonstrated enhanced specificity against PEDV M^{pro}. These compounds have potential as future therapeutics to combat PEDV infection.

INTRODUCTION

Porcine epidemic diarrhea virus (PEDV) is an enveloped, single strand, positive-sense RNA virus belonging to the genus *Alphacoronavirus* in the subfamily *Coronavirinae*.[1, 2] Unlike human coronaviruses, which cause respiratory diseases, including severe acute respiratory syndrome (SARS) and Middle East respiratory syndrome (MERS), PEDV infects the gastrointestinal tract in feeder pigs and fattening swine and causes porcine epidemic diarrhea (PED). PED symptoms include severe diarrhea, vomiting, and high rates of morbidity and mortality (approaching 100% in young piglets). Although the symptoms of PED are similar to the gastroenteritis caused by another coronavirus porcine transmissible gastroenteritis virus (TGEV), PEDV causes more severe disease and a higher death rate among nursing piglets. PEDV was initially identified in the early 1970s and had been mainly limited to Europe.[3, 4] However, since the 1990s, additional severe PEDV outbreaks have been reported in Asian countries, including South Korea and China, causing significant economic losses in these countries that heavily rely on pork as a food source.[5, 6] The first epidemic of PEDV infection in the United States was reported in 2013,[7] and a total of 3 etiological PEDV strains have been identified to date.[8] The epidemic quickly spread across the entire continent into Mexico and Canada and resulted in the deaths of over 8 million newborn piglets during a one year period[1]. Therefore, the global spread of PEDV has caused severe and dramatic negative economic impacts on the food industry.[9]

Vaccines against epidemic PEDV strains have been used in several countries with limited success.[10, 11] Through active vaccination of sows, piglets gain passive immunity through maternal antibody transfer via milk. However, the low to moderate efficacy of PEDV vaccines on the market, possibly caused by antigenic and genetic variation, underscores the need for effective antiviral therapeutics. Broad-spectrum antiviral agents such as ribavirin have been tested *in vitro*.[12, 13] The genome of PEDV is approximately 28 kb in length and contains a large 5' open reading frame (ORF1) and at least 5 smaller ORFs (ORF2−6) in the 3' end.[1, 2] ORF1 encodes two large polypeptides of the replicase machinery: pp1a, and through ribosomal frameshift, pp1ab. Both pp1a and pp1ab are co-translationally cleaved into 16 nonstructural proteins (Nsps) that are mediated by two proteases: the main protease (M^{pro}, also called Nsp5) and the papain-like protease (PLP or Nsp3).[14] Given its essential role in proteolytic processing in viral replication, M^{pro} is highly conserved in different coronavirus species at the levels of amino acid sequence and three dimensional structure.[15-18] Furthermore, the lack of a human homolog makes M^{pro} an ideal drug target, which has been explored in the pharmaceutical development against human coronaviruses such as SARS and MERS.[15, 19]

RESULTS AND DISCUSSION

Peptidomimetic inhibitors carrying a Michael acceptor warhead achieve optimal pharmaceutical activity against viral protease through mechanism-based irreversible inhibition.[15] In a previous study, we designed and evaluated a series of wide-spectrum inhibitors targeting the main proteases of coronaviruses;[19] however, their therapeutic efficacy for PEDV had not been explored. In the current study focusing on PEDV M^{pro}, we first used a potent

inhibitor, compound **1** (N3), designed in our previous work[19] as an initial structural scaffold for SARS studies. The α,β-unsaturated ester group in compound **1** is commonly used to irreversibly inactivate cysteine proteases. As shown in Figure 1, the Michael acceptor was positioned between the P1 and P1' sites of the peptidomimetic backbone, thus maximizing its electrophilic potential with the cysteine residue of the Cys-His catalytic dyad. Compound **1** carries a comparatively bulky lactam ring at the P1 site to accommodate the absolute requirement for a glutamine residue at the P1 position of almost all coronavirus M^{pro} substrates. Beyond the preservation of critical hydrogen bonds required for S1 recognition, the lactam ring also participates in multiple van der Waals interactions. An alkyl leucine side chain was included at the P2 site to accommodate the hydrophobic S2 pocket. The valine side chain at the P3 site is solvent-exposed, and the Ala side chain at the P4 position favors compound **1** to readily enter into the comparatively small S4 pocket. To enhance the binding affinity, an isoxazole group was incorporated at the P5 position to increase the van der Waals contacts with flanking residues at either side.

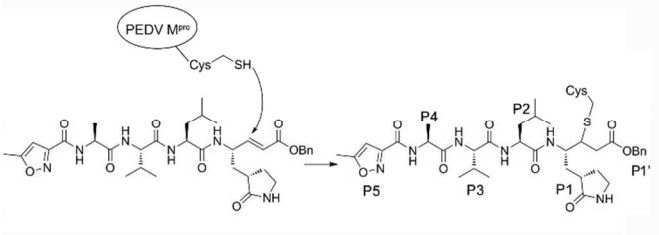

Figure 1. Scheme of Michael acceptor mediated irreversible inhibition of PEDV M^{pro}.

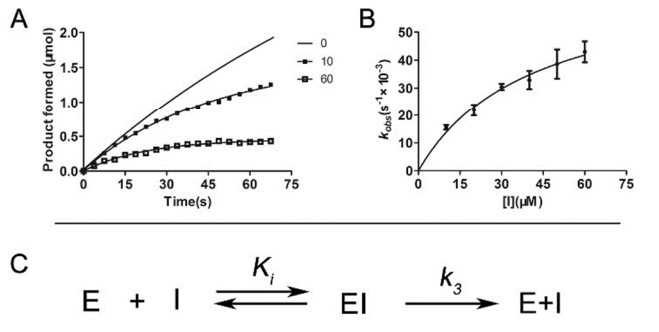

Figure 2. Inhibition of PEDV M^{pro} by compound **1** carrying a Michael acceptor warhead. (A) Reaction progress curves in the presence of increasing inhibitor concentration, indicating time-dependent inactivation of PEDV M^{pro}. (B) Plot of observed rate of inactivation constant (k_{obs}) over the concentration of compound **1**. A second-order inactivation rate constant was determined based on the plot. (C) Reaction scheme showing the two-step mechanism-based irreversible inactivation of PEDV M^{pro} by compound **1**.

To assess the efficacy of compound **1** on PEDV M^{pro}, time-dependent kinetic analyses were performed using a fluorescently labeled substrate, MCA-AVLQ↓SGFR-Lys(Dnp)-Lys-NH_2. Interestingly, the progress curves of compound **1** indicated time-dependent irreversible inhibition of PEDV M^{pro}, as the observed rate of inactivation (k_{obs}) increased with increasing concentration of the inhibitor (Figure 2A). Further, the hyperbolic shape of this curve (Figure 2B) supports the mechanism of two-step irreversible inactivation (Figure 2C). The inhibitor first forms a reversible complex with M^{pro} at the active site (EI) with a dissociation constant K_i; then, conjugate addition of the thiol group of Cys144 onto the Michael acceptor of compound **1** induces the formation of a covalent bond between M^{pro} and compound **1** (E–I). The K_i of compound **1** toward PEDV M^{pro} was determined to be 19.4 ± 0.7 μM. The rate constant, k_3, of Michael acceptor addition was determined to be 71.7 ± 4.2 10^{-3} s^{-1}, higher than 18.0 ± 1.1 10^{-3} s^{-1} of HCoV-229E and 3.1 ± 0.5 10^{-3} s^{-1} of SARS-CoV,[19] thus indicating a favorable conformation created in EI for covalent bond formation.

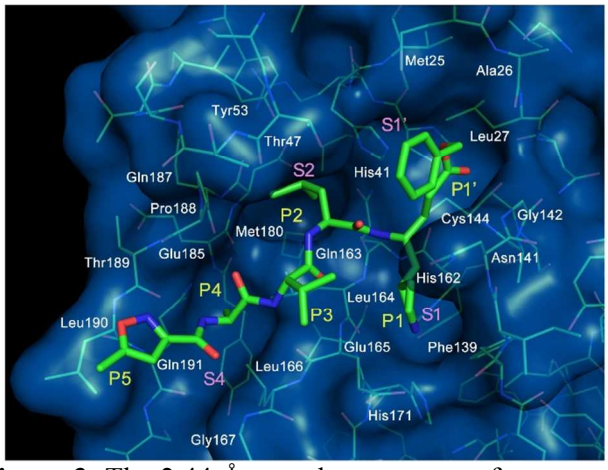

Figure 3. The 2.44 Å complex structure of compound **1** (colored green) bound to PEDV M^{pro} (PDB ID 5GWZ), indicating that **1** occupies the substrate-binding site.

The structure of PEDV M^{pro} dimer bound to compound **1** confirmed that the hypothesized mechanism-based irreversible inhibition occurred at the active site of the enzyme (Figure 3). Considering monomer A, for example, compound **1** is located at the cleft between domain I and II of PEDV M^{pro}, with a buried surface area of 706.4 $Å^2$ (approximately 72.3% of the total surface area) (Figure 4A and S3,

Supporting Information). A 1.83-Å C−S covalent bond was observed between the Cβ atom of vinyl group of compound **1** and the Sγ atom of Cys144, evidencing Michael acceptor addition (Figure 4B and S4, Supporting Information). Furthermore, compound **1** is stabilized by a network of 8 hydrogen bonds involving the Nε2 atom of His162; the carbonyl group of Gln163, Glu165, and Thr189; the amide nitrogen of Cys144 and Glu165; and the Oε2 atom of Glu165 (Figure 4B and Table S2, Supporting Information). In addition, as shown in Figure 3, the P1 and P2 subsites of compound **1** insert favorably into S1 (consisting of residues Phe139−Asn141, Cys144, His162−Glu165, and His171) and S2 (consisting of His41, Thr47, Tyr53, Gln163−Leu164, Met180, and Glu185−Pro188) substrate-binding pockets, respectively. The P3 site of **1** is solvent facing, while the P4 and P5 sites are accommodated by one loop formed by residues 188−191 and another loop/strand spanning residues 165−167. Structural comparison of the compound **1**-complex structure with similar inhibitor-protease structures from other coronaviruses including SARS-CoV,[19] HCoV-NL63,[18] HCoV-HKU1,[17] and TGEV[19] is shown in Figure S5, Supporting Information. Clearly, compound **1** adopts a similar binding mode in the substrate-binding pocket of PEDV M^{pro} compared with other CoV M^{pro}-compound **1** complex structures. The differences lie in the orientations of P5 and P1′. One possibility is that subsites S5 and S1′ in CoV M^{pro}s are very shallow, making P5 and P1′ partially solvent exposed. Thus, strong interactions are not readily achieved at these two subsites.

The above structural data based on lead compound **1** permitted further rational optimization of a Michael acceptor-based peptidomimetic inhibitor to target the substrate-binding pocket of PEDV M^{pro}. We then designed a series of 17 new compounds derived from the backbone structure of compound **1** with altered side chains (Table S3, Supporting Information). Briefly, in the molecular design, we kept the lactam ring at P1 and the side chain of Leu at P2, but replaced P3, P4, P5 and P1′ with various functional groups to obtain lead compounds with better inhibition. Specifically, in the newly synthesized compound **3** (M2), the P3 site is a cyclopentane; in compound **15** (M17), the P1′ site is a fluoride-substituted benzyl ester.[20]

To screen for improved inhibitory activity of these 17 newly designed compounds, we determined the percentage inactivation of the initial enzymatic activity of PEDV M^{pro} (defined as the initial slope of the reaction curve). As shown in Table 1, compound **1** was used as the reference, which achieved 89% inhibition of PEDV M^{pro}. Two of the new compounds, **3** and **15** (Table S3, Supporting Information), achieved much better inhibitory activity than compound **1**, with percentage inactivation of PEDV M^{pro} as 96% and 93%, respectively. The K_i parameters of compounds **3** and **15** toward PEDV M^{pro} were determined to be 7.1 ± 0.2 μM and 8.3 ± 0.3 μM, respectively (Figure S6, Supporting Information), which demonstrated improved activity compared with that of compound **1**. The rate constant k_3 of Michael acceptor addition for compounds **3** and **15** was determined to be 59.2 ± 2.8 10^{-3} s^{-1} and 66.7 ± 2.7 10^{-3} s^{-1}, respectively (Figure S6, Supporting Information), both of which remained at the same level with compound **1**, but much higher than the k_3 rate constant for other coronaviruses. Therefore, the two newly designed compounds, **3** and **15**, demonstrated improved inhibitory specificity towards PEDV M^{pro} compared to the lead compound **1**.

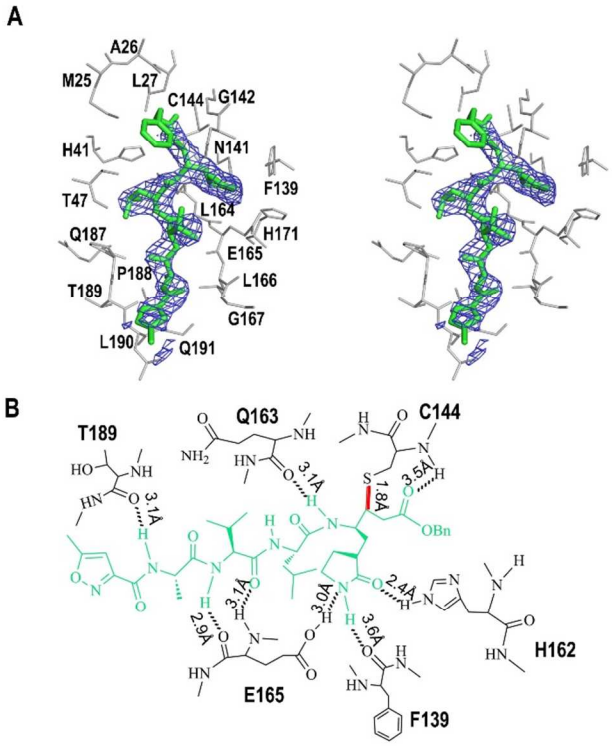

Figure 4. Graphical representation demonstrating the key interactions between compound **1** and PEDV M^{pro} (PDB ID 5GWZ). (A) Interaction between compound **1** and PEDV M^{pro}. (B) Detailed view of key covalent and hydrogen bonds between compound **1** and PEDV M^{pro}.

CONCLUSION

In summary, we have presented the application of Michael acceptor-based peptidomimetic small molecule inhibitor to target PEDV M^{pro}, an essential and conserved enzyme in the viral replication. We obtained the co-crystal structure of wide-spectrum

compound **1** bound to PEDV M^{pro}, revealing the detailed irreversible inhibition mechanism at the active site of the enzyme. Based on this structure, we further designed and synthesized another series of 17 inhibitors with altered side groups. Two compounds, **3** and **15**, demonstrated improved inhibitory activity against PEDV M^{pro}, particularly with improved affinity for the active site as demonstrated by the much lower K_i. Therefore, the class of peptidomimetic inhibitor carrying a Michael acceptor has the potential to enter pharmaceutical development as a promising therapeutic to treat acute gastroenteritis in pigs and especially nursing piglets infected by PEDV.

Table 1. Evaluation of the inhibitor activity targeting PEDV M^{pro} for compound 1 and the 17 newly synthesized compounds. Inhibition ratio (Ir) is defined as the percentage inactivation of the initial enzymatic activity of PEDV M^{pro}.

compound	Inhibition ratio (Ir)	Inhibitory activity[a]
1	89%	++++
2	87%	++++
3	96%	+++++
4	80%	+++
5	-	N/A[b]
6	12%	+
7	72%	+++
8	10%	+
9	62%	++
10	75%	+++
11	20%	+
12	-	N/A
13	-	N/A
14	80%	+++
15	93%	+++++
16	90%	++++
17	89%	++++
18	90%	++++

[a]Percentage inhibitory activity: +++++, >90%; ++++, 80%−90%; +++, 70%−80%; ++, 20%−70%; +, <20%. [b]No inhibition was observed.

EXPERIMENTAL SECTION

Structure Determination and Analysis

The structure of the PEDV M^{pro}-compound **1** complex was determined using molecular replacement from that of HCoV-229E M^{pro} (PDB entry 2ZU2). All cross-rotation and translation searches for molecular replacement were performed with Phaser.[21] Cycles of manual adjustment using Coot[22] and subsequent refinement using PHENIX[23] led to a final model with a crystallographic R factor (R_{cryst}) of 18.5% and a free R factor (R_{free}) of 21.9% at 2.44-Å resolution. All parameters of X-ray data processing and refinement are detailed in Table S1, Supporting Information. A summary of the covalent bond and all hydrogen bonds between PEDV M^{pro} and compound **1** are listed in Table S2, Supporting Information.

Enzymatic Activity and Inhibition Assays

Enzymatic assays were performed using a fluorogenic substrate with a consensus sequence of CoVMpro, MCA-AVLQ↓SGFR-Lys(Dnp)-Lys-NH2 (>95% purity, GL Biochem Shanghai Ltd., Shanghai, China), as previously reported.[16, 17, 19] Fluorescence intensity was monitored using a Fluoroskan Ascent instrument (Thermo Scientific, USA) with excitation and emission wavelengths of 320 and 405 nm, respectively. The assay was performed in a buffer solution consisted of 50 mM Tris-HCl (pH 7.3) and 1 mM EDTA at 30 °C. Kinetic parameters, including K_m and k_{cat} of PEDV M^{pro} (Figure S1 and S2, Supporting Information) and K_i and k_3 of the inhibitors,[17, 19] were determined using methods described in detail in the Supporting Information.

Chemical Synthesis of Compounds 3 and 15

The synthetic pathway of compound **3** was detailed in Supporting Information, which was similar to that of compound **1**.[19] Compound **15** was synthesized from **1**: 7 mg LiOH was added to a solution of compound **1** (0.1 g) in 3 mL THF, and water was added until the solution became clear. Then it was stirred for 1 hour. After completion of the reaction, 1 M HCl (*aq*) was add to adjust the pH to 3; then, the solvent was evaporated and purification followed to yield a white solid (0.06 g), which was then dissolved in 1 mL DMF, with 1-(1-bromoethyl)-2-fluorobenzene (41 mg) and 34 μL DIEA. The solution was stirred overnight, and after completion of the reaction, DMF was removed, and the residue was purified by silica gel chromatography to yield compound **15**. Both compounds **3** and **15** were further purified using preparative HPLC.

Characterization of Compounds.

All compounds used in this study (Table 1) were characterized with ^{1}H and ^{13}C NMR spectroscopy, ESI-MS, and HPLC. The purity of all compounds was > 95% according to analytical HPLC using UV detection at 215 nm. All data for compound characterization are provided in Supporting Information.

ASSOCIATED CONTENT

Supporting Information

The Supporting Information is available free of charge on the ACS Publications website at DOI:

Enzymatic activity of PEDV M^{pro}, structural overview and comparison of PEDV M^{pro}-compound **1** interaction, inhibition kinetics of compounds **3** and **15**, X-ray data collection and refinement statistics, details and characterization data including purity for all 17 compounds, additional methods (PDF)

PDB coordinates for complex structure of PEDV M^{pro} with compound **1** (PDB)

Molecular formula strings and some data (CSV)

Accession Codes

Atomic coordinates for the crystal structure of PEDV M^{pro} in complex with compound **1** can be accessed using PDB ID 5GWZ. Authors will release the atomic coordinates and experimental data upon article publication.

AUTHOR INFORMATION

Corresponding Authors

*H.Y.: phone, +86 22 27403906; fax, +86 22 27403902; e-mail, yanght@tju.edu.cn.

*C.Y.: phone, +86 22 65378009; fax, +86 22 65378036; e-mail, caiyan_86@163.com.

Author Contributions

[+]F.W., C.C., and K.Y. contributed equally and are considered as co-first authors. All authors have given approval to the final version of this manuscript.

Notes

The authors declare no competing financial interest.

ACKNOWLEDGEMENTS

We thank Dunquan Jiang for data collection at beamline BL-5A (the Photon Factory, KEK, Japan) and Steve C. Ding for helpful discussion. This work was supported by the National Key Basic Research Program of China (973 program, grant 2015CB859800), the Binhai New Area Special Fund for Innovations in Science and Technology, the National Natural Science Foundation of China (grant 31528006), the National Key Research Program of China (No. 2016YFD0500300), and the Tianjin Marine Science and Technology Program (grant KJXH2014-16).

ABBREVIATIONS USED

PED, porcine epidemic diarrhea; PEDV, Porcine Epidemic Diarrhea Virus; M^{pro}, main protease; SARS, severe acute respiratory syndrome; MERS, Middle East respiratory syndrome.

REFERENCES

1. Lee, C. Porcine epidemic diarrhea virus: An emerging and re-emerging epizootic swine virus. *Virol. J.* **2015,** *12*, 193.

2. Song, D.; Park, B. Porcine epidemic diarrhoea virus: a comprehensive review of molecular epidemiology, diagnosis, and vaccines. *Virus Genes* **2012,** *44*, 167-175.

3. Chasey, D.; Cartwright, S. F. Virus-like particles associated with porcine epidemic diarrhoea. *Res. Vet. Sci.* **1978,** *25*, 255-256.

4. Wood, E. N. An apparently new syndrome of porcine epidemic diarrhoea. *Vet. Rec.* **1977,** *100*, 243-244.

5. Li, W.; Li, H.; Liu, Y.; Pan, Y.; Deng, F.; Song, Y.; Tang, X.; He, Q. New variants of porcine epidemic diarrhea virus, China, 2011. *Emerging Infect. Dis.* **2012,** *18*, 1350-1353.

6. Sun, R. Q.; Cai, R. J.; Chen, Y. Q.; Liang, P. S.; Chen, D. K.; Song, C. X. Outbreak of porcine epidemic diarrhea in suckling piglets, China. *Emerging Infect. Dis.* **2012,** *18*, 161-163.

7. Stevenson, G. W.; Hoang, H.; Schwartz, K. J.; Burrough, E. R.; Sun, D.; Madson, D.; Cooper, V. L.; Pillatzki, A.; Gauger, P.; Schmitt, B. J.; Koster, L. G.; Killian, M. L.; Yoon, K. J. Emergence of porcine epidemic diarrhea virus in the United States: clinical signs, lesions, and viral genomic sequences. *J. Vet. Diagn. Invest.* **2013,** *25*, 649-654.

8. Marthaler, D.; Bruner, L.; Collins, J.; Rossow, K. Third strain of porcine epidemic diarrhea virus, United States. *Emerging Infect. Dis.* **2014,** *20*, 2162-2163.

9. Schulz, L. L.; Tonsor, G. T. Assessment of the economic impacts of porcine epidemic diarrhea virus in the United States. *J. Anim. Sci.* **2015,** *93*, 5111-5118.

10. Kweon, C. H.; Kwon, B. J.; Lee, J. G.; Kwon, G. O.; Kang, Y. B. Derivation of attenuated porcine epidemic diarrhea virus (PEDV) as vaccine candidate. *Vaccine* **1999,** *17*, 2546-2553.

11. Song, D. S.; Oh, J. S.; Kang, B. K.; Yang, J. S.; Moon, H. J.; Yoo, H. S.; Jang, Y. S.; Park, B. K. Oral efficacy of Vero cell attenuated porcine epidemic diarrhea virus DR13 strain. *Res. Vet. Sci.* **2007,** *82*, 134-140.

12. Kim, S. H.; Lee, J. M.; Jung, J.; Kim, I. J.; Hyun, B. H.; Kim, H. I.; Park, C. K.; Oem, J. K.; Kim, Y. H.; Lee, M. H.; Lee, K. K. Genetic characterization of porcine epidemic diarrhea virus in Korea from 1998 to 2013. *Arch. Virol.* **2015,** *160*, 1055-1064.

13. Lee, D. K.; Park, C. K.; Kim, S. H.; Lee, C. Heterogeneity in spike protein genes of porcine epidemic diarrhea viruses isolated in Korea. *Virus Res.* **2010,** *149*, 175-182.

14. Brian, D. A.; Baric, R. S. Coronavirus genome structure and replication. *Curr. Top. Microbiol. Immunol.* **2005,** *287*, 1-30.

15. Yang, H.; Bartlam, M.; Rao, Z. Drug design targeting the main protease, the Achilles' heel of coronaviruses. *Curr. Pharm. Des.* **2006,** *12*, 4573-4590.
16. Xue, X.; Yu, H.; Yang, H.; Xue, F.; Wu, Z.; Shen, W.; Li, J.; Zhou, Z.; Ding, Y.; Zhao, Q.; Zhang, X. C.; Liao, M.; Bartlam, M.; Rao, Z. Structures of two coronavirus main proteases: implications for substrate binding and antiviral drug design. *J. Virol.* **2008,** *82*, 2515-2527.
17. Zhao, Q.; Li, S.; Xue, F.; Zou, Y.; Chen, C.; Bartlam, M.; Rao, Z. Structure of the main protease from a global infectious human coronavirus, HCoV-HKU1. *J. Virol.* **2008,** *82*, 8647-8655.
18. Wang, F.; Chen, C.; Tan, W.; Yang, K.; Yang, H. Structure of main protease from human coronavirus NL63: insights for wide spectrum anti-coronavirus drug design. *Sci. Rep.* **2016,** *6*, 22677.
19. Yang, H.; Xie, W.; Xue, X.; Yang, K.; Ma, J.; Liang, W.; Zhao, Q.; Zhou, Z.; Pei, D.; Ziebuhr, J.; Hilgenfeld, R.; Yuen, K. Y.; Wong, L.; Gao, G.; Chen, S.; Chen, Z.; Ma, D.; Bartlam, M.; Rao, Z. Design of wide-spectrum inhibitors targeting coronavirus main proteases. *PLoS Biol.* **2005,** *3*, e324.
20. Rao, Z.; Yang, H.; Fu, S.; Yang, C.; Wang, Z.; Cai, Y.; Li, S.; Guo, Y.; Liu, H. Small molecule inhibitors of coronavirus main protease: their preparation and application. China Patent 201510079787, Feb 15, 2015.
21. McCoy, A. J.; Grosse-Kunstleve, R. W.; Adams, P. D.; Winn, M. D.; Storoni, L. C.; Read, R. J. Phaser crystallographic software. *J. Appl. Crystallogr.* **2007,** *40*, 658-674.
22. Emsley, P.; Cowtan, K. Coot: model-building tools for molecular graphics. *Acta Crystallogr. Sect. D Biol. Crystallogr.* **2004,** *60*, 2126-2132.
23. Adams, P. D.; Afonine, P. V.; Bunkoczi, G.; Chen, V. B.; Davis, I. W.; Echols, N.; Headd, J. J.; Hung, L. W.; Kapral, G. J.; Grosse-Kunstleve, R. W.; McCoy, A. J.; Moriarty, N. W.; Oeffner, R.; Read, R. J.; Richardson, D. C.; Richardson, J. S.; Terwilliger, T. C.; Zwart, P. H. PHENIX: a comprehensive Python-based system for macromolecular structure solution. *Acta Crystallogr. Sect. D Biol. Crystallogr.* **2010,** *66*, 213-221.

Table of Contents Graphic:

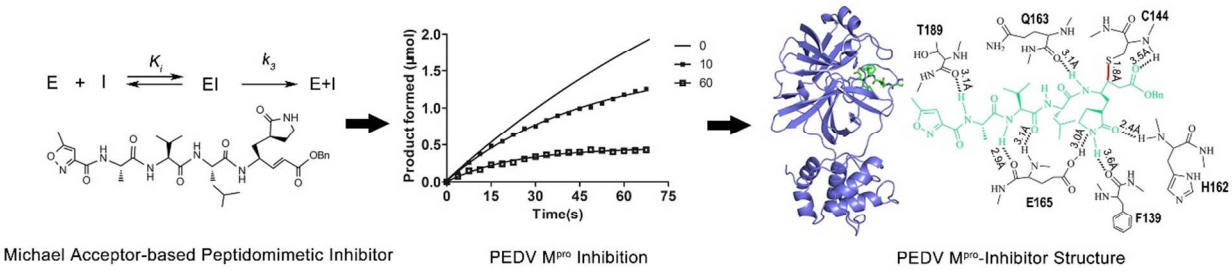

Michael Acceptor-based Peptidomimetic Inhibitor

PEDV M^{pro} Inhibition

PEDV M^{pro}-Inhibitor Structure

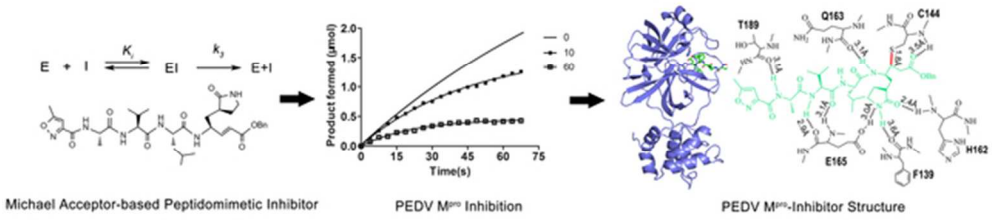

PEDV_toc

54x14mm (300 x 300 DPI)

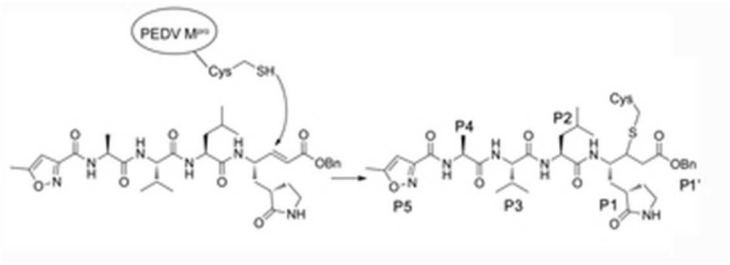

PEDV_fig1

30x10mm (300 x 300 DPI)

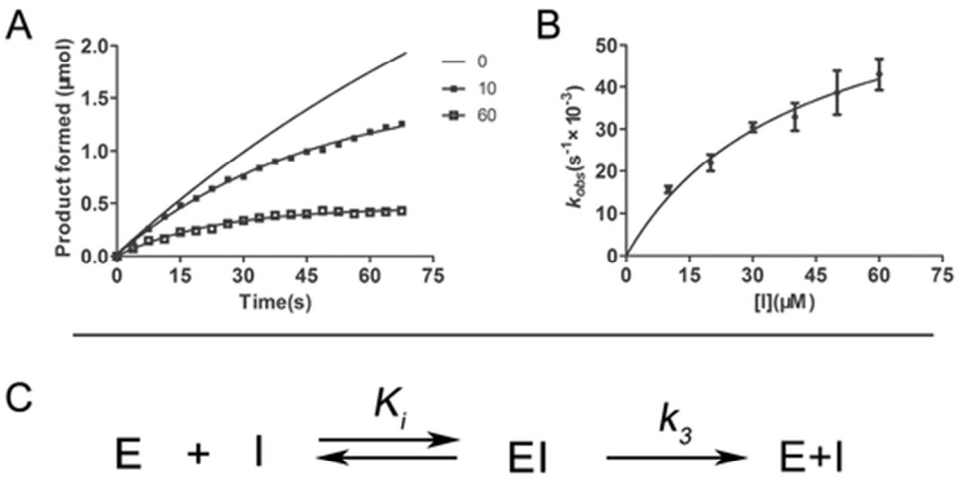

PEDV_fig2

47x28mm (300 x 300 DPI)

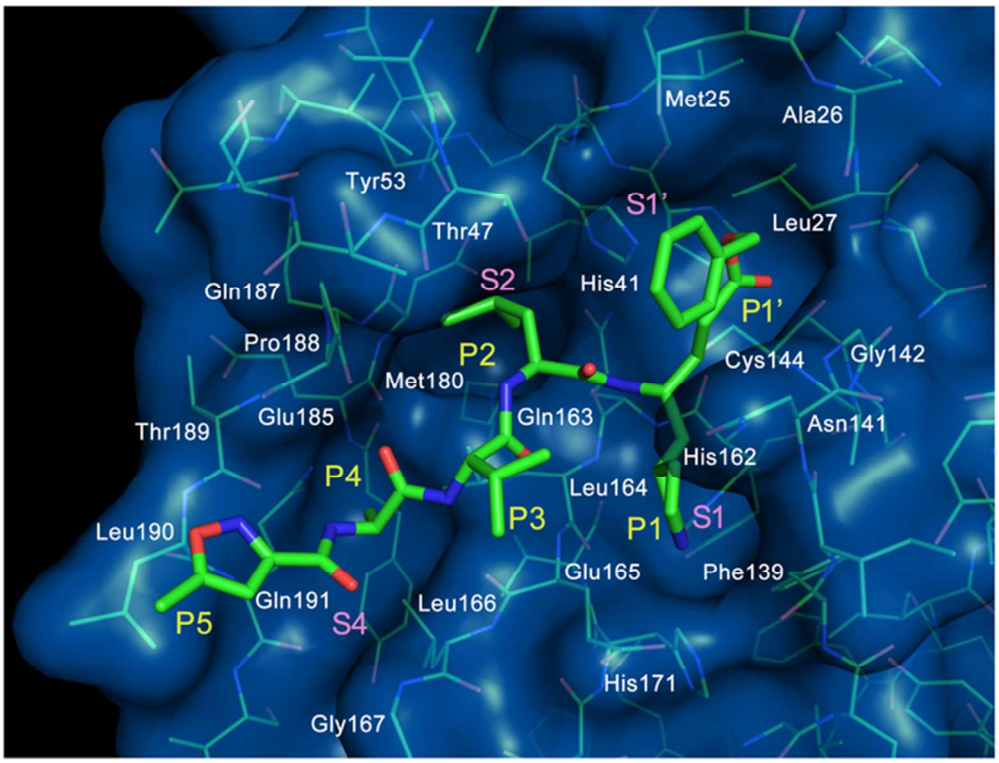

PEDV_fig3

60x45mm (300 x 300 DPI)

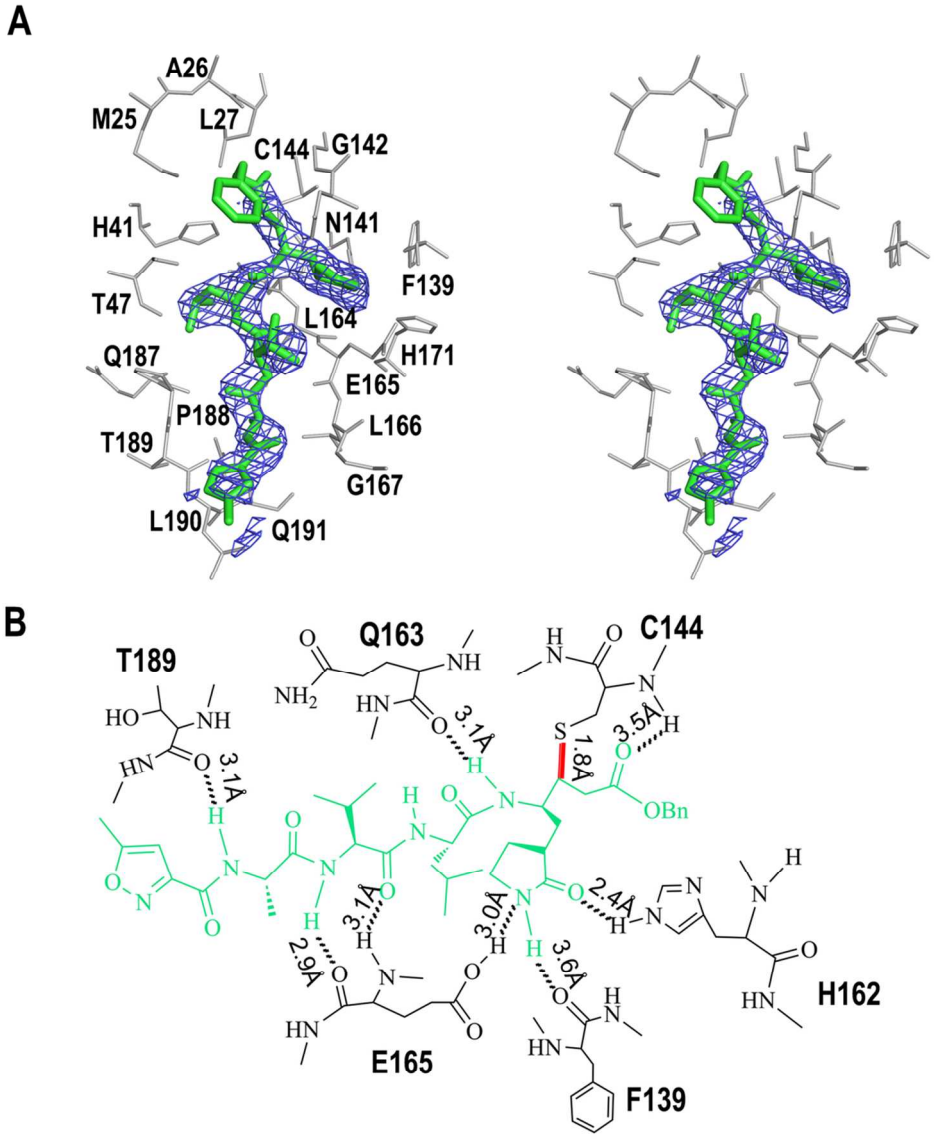

PEDV_fig4

103x124mm (300 x 300 DPI)